© 2020. Published by The Company of Biologists Ltd | Journal of Cell Science (2020) 133, jcs241836. doi:10.1242/jcs.241836

SHORT REPORT

Cep57 and Cep57l1 function redundantly to recruit the Cep63–Cep152 complex for centriole biogenesis

Huijie Zhao[1,*], Sen Yang[1,2,*], Qingxia Chen[1,2,3], Xiaomeng Duan[1], Guoqing Li[1], Qiongping Huang[1], Xueliang Zhu[1,2,3,‡] and Xiumin Yan[1,‡]

ABSTRACT

The Cep63–Cep152 complex located at the mother centriole recruits Plk4 to initiate centriole biogenesis. How the complex is targeted to mother centrioles, however, is unclear. In this study, we show that Cep57 and its paralog, Cep57l1, colocalize with Cep63 and Cep152 at the proximal end of mother centrioles in both cycling cells and multiciliated cells undergoing centriole amplification. Both Cep57 and Cep57l1 bind to the centrosomal targeting region of Cep63. The depletion of both proteins, but not either one, blocks loading of the Cep63–Cep152 complex to mother centrioles and consequently prevents centriole duplication. We propose that Cep57 and Cep57l1 function redundantly to ensure recruitment of the Cep63–Cep152 complex to the mother centrioles for procentriole formation.

KEY WORDS: Centriole, Centriole duplication, Cep57, Cep57l1, Cep63, Cep152

INTRODUCTION

In mammalian cells, centrosomes function as spindle poles in mitosis and basal bodies for cilia formation. Typically, a centrosome is made of two cylindrical centrioles surrounded by pericentriolar material (PCM) (Nigg and Raff, 2009). In dividing animal cells, the duplication of centrioles must be tightly controlled with only a procentriole (herein referred to as daughter centriole) forming next to each of the two pre-existing centrioles (mother centrioles) per cell cycle to ensure the correct bipolar spindle formation, which is important for the integrity of the genome. Aberration in centriole duplication is commonly present in numerous tumors and other diseases (Bettencourt-Dias et al., 2011; Gönczy, 2015; Nigg and Holland, 2018). In recent years, great progress has been made in the understanding of the molecular mechanisms of centriole biogenesis. To initiate centriole duplication in mammals, Plk4 is firstly recruited by the Cep192-containing ring around the proximal mother centrioles at the early G1 phase and subsequently translocated to the larger Cep152-containing ring when Cep152 is recruited to the mother centriole (Kim et al., 2013; Sonnen et al., 2013). At the Cep152 ring, Plk4 recruits and phosphorylates Stil (also known as SAS-5 in *Caenorhabditis elegans*) to load Sas-6 for cartwheel formation (Arquint et al., 2015, 2012; Cizmecioglu et al., 2010; Dzhindzhev et al., 2010; Moyer et al., 2015; Ohta et al., 2014, 2018). Several proteins, including Cep135, Cpap (also known as CENPJ), Cp110 (CCP110) and Cep120, contribute to building the centriolar microtubule (MT) wall and mediate centriole elongation (Azimzadeh and Marshall, 2010; Brito et al., 2012; Carvalho-Santos et al., 2012; Comartin et al., 2013; Hung et al., 2004; Kohlmaier et al., 2009; Lin et al., 2013a,b; Loncarek and Bettencourt-Dias, 2018; Schmidt et al., 2009). It is known that Cep152 is recruited by Cep63 to act as the cradle for the mother centriole-dependent (MCD) centriole biogenesis (Brown et al., 2013; Kim et al., 2019; Sir et al., 2011; Zhao et al., 2013). However, it is still unclear how Cep63 or a Cep63–Cep152 complex is targeted to the proximal end of mother centrioles.

Cep57, an FGF-2 binding and trafficking protein, has been reported to be required for normal centriole duplication, proper chromosome segregation, PCM organization and centriole engagement (Bossard et al., 2003; Cuevas et al., 2013; Meunier et al., 2009; Snape et al., 2011; Watanabe et al., 2019; Wu et al., 2012; Zhou et al., 2016). Cep57, Cep63 and Cep152 form a stable complex at the proximal end of the centrioles, and Cep57 is a proximity interactor of Cep63 (Firat-Karalar et al., 2014; Lukinavičius et al., 2013; Sieben et al., 2018), suggesting that Cep57 may be involved in the centriolar targeting of the Cep63–Cep152 complex for centriole duplication.

In this study, we find that Cep57 and its paralog Cep57l1 function redundantly to recruit the Cep63–Cep152 complex for centriole duplication.

RESULTS AND DISCUSSION

Cep57 specifically colocalizes with Cep63 and Cep152 at the proximal end of mother centrioles

To investigate the spatial relationship of Cep57, Cep63 and Cep152, we co-stained Cep57 with either Cep63 or Cep152 in U2OS cells. Consistent with results from the previous study (Lukinavičius et al., 2013), 3D-structured illumination microscopy (3D-SIM) results showed that Cep57 formed a ring-like structure with Cep63 and Cep152 at the proximal end of both centrioles (Fig. 1A). Cep57 colocalized with Cep63 in rings of a similar diameter (Fig. 1A,B). Consistent with this, GFP–Cep57 was also enriched at the base of mother centrioles in U2OS cells. In addition to the centriolar localization, overexpressed GFP–Cep57 forms bundled filaments in the cytoplasm (Momotani et al., 2008; Wu et al., 2012; Zhou et al., 2016), and both Cep63 and Cep152 were recruited to these filaments (Fig. 1C,D), indicating that Cep57, Cep63 and Cep152 form a complex, and Cep57 could recruit Cep63 and Cep152 *in vivo*.

During multiciliation, mouse tracheal epithelial cells (mTECs) assemble hundreds of centrioles through both MCD and deuterosome-dependent (DD) pathways, respectively driven by Cep63 and its paralog Deup1 (Zhao et al., 2019, 2013). Cep152 localizes to both

[1]State Key Laboratory of Cell Biology, Shanghai Institute of Biochemistry and Cell Biology, Center for Excellence in Molecular Cell Science, Chinese Academy of Sciences, Shanghai 200031, China. [2]University of Chinese Academy of Sciences, Beijing 100049, China. [3]School of Life Science and Technology, ShanghaiTech University, 100 Haike Road, Shanghai 201210, China.
*These authors contributed equally to this work

‡Authors for correspondence (yanx@sibcb.ac.cn; xlzhu@sibcb.ac.cn)

H.Z., 0000-0002-8595-8159; X.Z., 0000-0001-8019-9336; X.Y., 0000-0002-3260-1690

Handling Editor: David Glover
Received 22 November 2019; Accepted 27 May 2020

Journal of Cell Science (2020) 133, jcs241836. doi:10.1242/jcs.241836

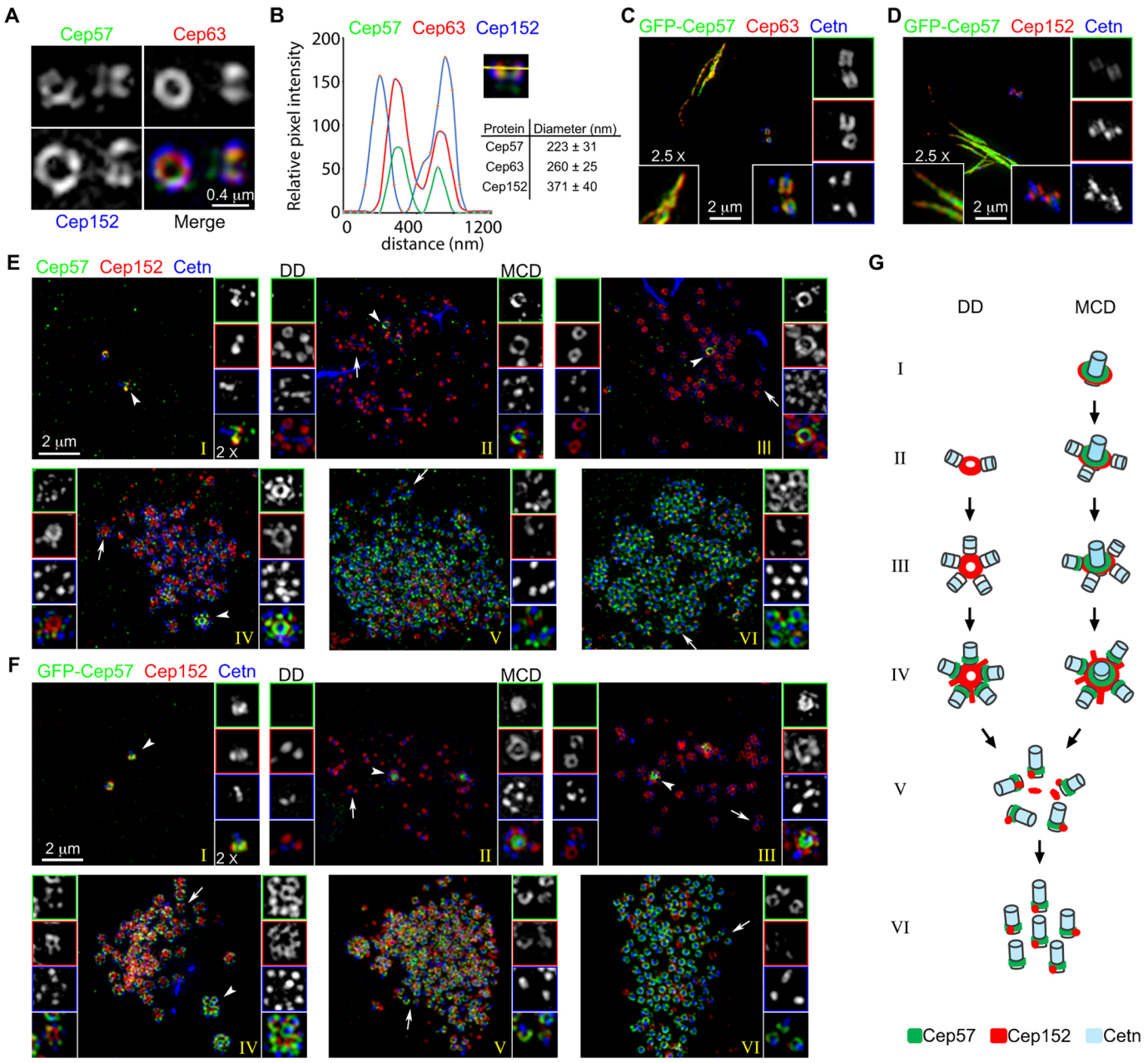

Fig. 1. Cep57 colocalizes with Cep63 and Cep152 at the proximal end of centrioles. (A) Cep57 colocalizes with Cep63 and Cep152. Cep57 (green) was co-stained with Cep63 (red) and Cep152 (blue) in human U2OS cells. (B) The line intensity plot shows the centriolar colocalization of Cep57, Cep63 and Cep152. The distance between the two peaks of the Gaussian curve was measured and considered as the diameter; 26 centrioles from 13 cells were scored. Mean±s.d. values are presented. (C,D) Cep63 and Cep152 are recruited to the bundled filaments of GFP–Cep57 in U2OS cells. U2OS cells transfected with GFP–Cep57 for 48 h were pre-extracted with 0.5% Triton X-100 for 40 s and fixed to stain for centrin (Cetn, blue) and Cep63 (red) or Cep152 (red). (E,F) Cep57-specified MCD cradles during centriole amplification in mTECs. mTECs (E) or mTECs expressing GFP–Cep57 (F) were fixed at day 3 after inducing multiciliation with the air-liquid interface system (ALI d3) and stained for Cep152 (red), Cetn (blue) and Cep57 (green) or GFP. Cep152 serves as a marker of both the mother centriole and deuterosome, and centrin as the marker of centrioles. Representative 3D-SIM images in the indicated stages of centriole amplification are presented. Magnified areas are used to show details for the MCD (right; arrowheads) and DD (left; arrows) centriole amplification. (G) Schematic illustration models are presented to aid understanding.

parental centrioles and deuterosomes but Cep63 only displays parental centriole localization (Zhao et al., 2013). Interestingly, Cep57 behaved similarly to Cep63 at the early stages of the centriole amplification. It colocalized with Cep152 at the proximal ends of parental centrioles from stage I but showed no deuterosome localization in stages II and III (Fig. 1E–G). In stage IV, Cep57 started to occupy the base of procentrioles formed around the parental centrioles and deuterosomes. In stages V and VI, Cep57 persistently localized to the proximal ends of nascent centrioles as a full ring structure (Fig. 1E–G), while Cep152 and Cep63 displayed as a dot (Zhao et al., 2013). Therefore, Cep57 only contributes to the MCD pathway and could recruit Cep152 to parental centrioles together with Cep63.

Cep57, Cep63 and Cep152 interact hierarchically

To explore the relationship among Cep57, Cep63 and Cep152, we performed co-immunoprecipitation and GST pulldown experiments

Journal of Cell Science (2020) 133, jcs241836. doi:10.1242/jcs.241836

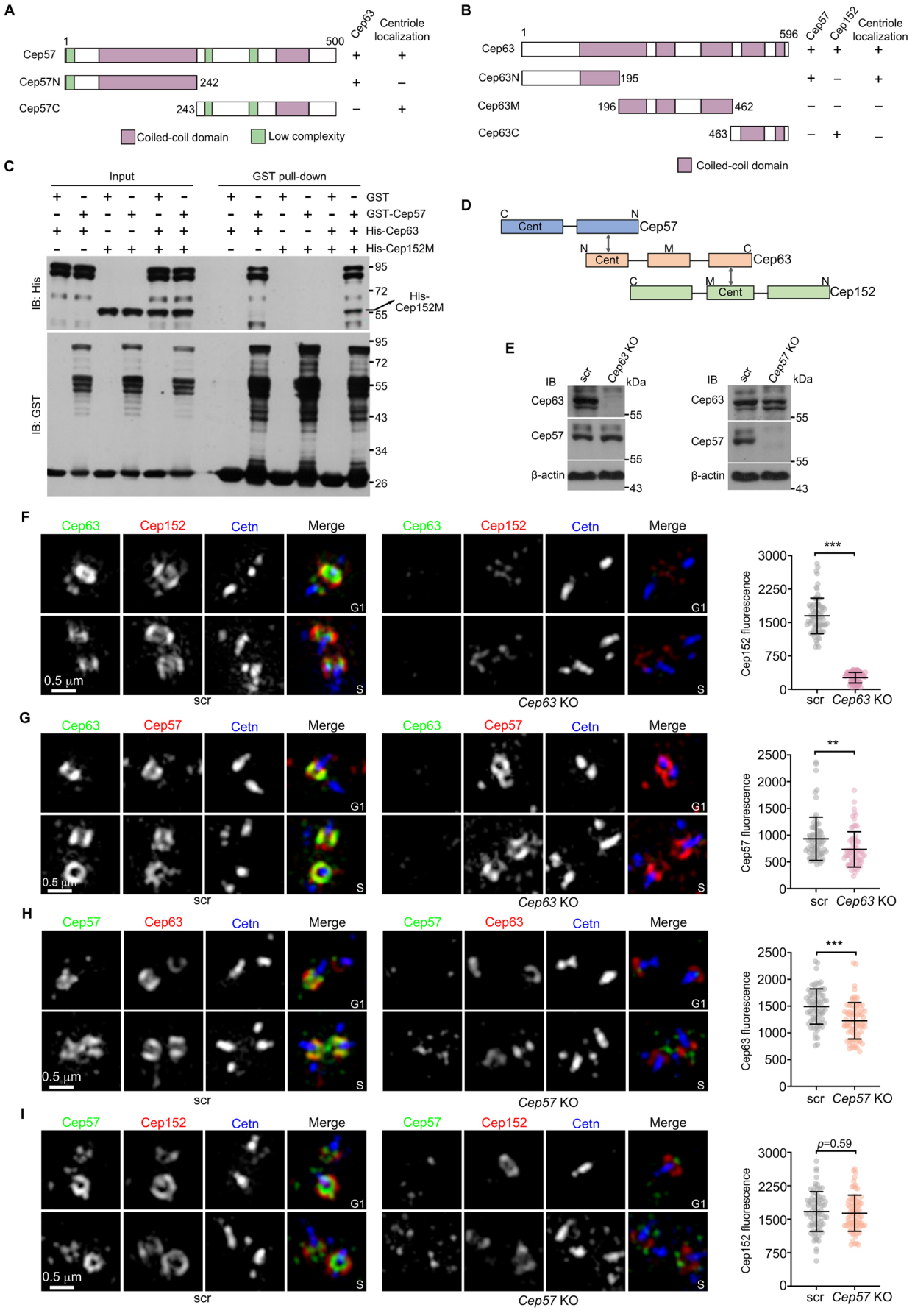

Fig. 2. See next page for legend.

Fig. 2. Cep57 directly interacts with Cep63, but is dispensable for centriolar anchoring of the Cep63–Cep152 complex. (A) Mapping the Cep63-interacting regions of Cep57. The numbers indicate amino acid positions. The N-terminus of Cep57 is required for the interaction with Cep63 and the C-terminus for its centrosomal localization. (B) Domain mapping of Cep63. The numbers indicate amino acid positions. The N-terminus of Cep63 is required for the interaction with Cep57 and its centrosomal localization, whereas the C-terminus interacts with Cep152 (Zhao et al., 2013). (C) GST pulldown assay. Bacterial lysates expressing the indicated proteins were mixed and subjected to GST pulldown assays. Cep152M contains the fragment of mouse Cep152 from positions 1075 to 1383 aa (Zhao et al., 2013). (D) Schematics showing the interaction order of Cep57, Cep63 and Cep152. Cent represents the centrosomal-targeting region. (E) Confirmation of the KO cell lines. *Cep57* or *Cep63* knockout (KO) U2OS cells were lysed and subjected to immunoblotting. β-actin served as the loading control. (F,G) The effects of knockout of *Cep63* on the centrosomal localization of Cep152 (F) or Cep57 (G) in U2OS cells. Note that knockout of *Cep63* significantly reduced the centrosomal localization of Cep152, but not Cep57. (H,I) The effects of knockout of *Cep57* on the centrosomal localization of Cep63 (H) or Cep152 (I) in U2OS cells. Note that both Cep63 and Cep152 still localized to the centrioles upon the *Cep57* depletion. Quantification results (F–I) were from three independent experiments, and 75 cells at the G1 phase were scored per condition. Mean±s.d. values are presented in the plots. $^{**}P<0.01$, $^{***}P<0.001$ (Student's *t*-test).

(Fig. 2; Fig. S1). Cep57 localized to the centriole via its C-terminal MT-binding domain (Momotani et al., 2008) and interacted with Cep63 through its N-terminal coiled-coil domain (Fig. 2A; Fig. S1A,B). Cep63 bound to Cep57 via its N-terminal centriole-binding region, and its C-terminus interacted with the centrosomal-targeting region of Cep152 (152M) (Fig. 2B; Fig. S1C,D) (Hatch et al., 2010; Zhao et al., 2013). In the GST pulldown assay, GST–Cep57 directly interacted with His–Cep63, but could not pull down Cep152M in the absence of Cep63 (Fig. 2C), indicating that Cep57 forms the complex with Cep152 through Cep63 and these three proteins interact in a hierarchical manner (Fig. 2D). These results indicate that Cep57 localizes to the proximal mother centriole through its C-terminus and recruits the Cep63–Cep152 complex by directly binding to the centriolar targeting region of Cep63.

Depletion of Cep57 does not abolish the centriolar localization of Cep63 and Cep152

To test whether Cep57 is required for the centrosomal targeting of Cep63 and Cep152, we generated *Cep57* and *Cep63* knockout (KO) U2OS cell lines using the CRISPR/Cas9 method (Fig. 2E; Fig. S2A,B) (Cong et al., 2013). Consistent with previous studies (Brown et al., 2013; Sir et al., 2011), bipolar spindle formation and centriole duplication were mildly affected by the depletion of Cep63 (Fig. S2C–E). Immunofluorescence analysis of *Cep63* KO or *Cep57* KO cell lines revealed a complete loss of Cep63 or Cep57 ring-like signals at the proximal end of centrioles (Fig. 2F–I). As reported previously (Lukinavičius et al., 2013; Sir et al., 2011), the Cep152 centrosomal signal was reduced dramatically in *Cep63* KO cells compared to that in control cells (Fig. 2F). The centrosomal localization of Cep57 was slightly affected in *Cep63* KO cells (Fig. 2G). Surprisingly, both Cep63 and Cep152 were still able to localize at the centrosome in *Cep57* KO cells (Fig. 2H–I). These results are in accordance with previous findings showing that Cep63 is essential for Cep152 centrosomal localization, whereas Cep57 seems to be dispensable for loading the Cep63–Cep152 complex to the centrosome (Lukinavičius et al., 2013; Sir et al., 2011).

The dispensable role of Cep57 in the centriolar targeting of the Cep63–Cep152 complex is contradictory to the fact that Cep57 forms a stable complex with Cep63 and Cep152 by directly binding to the centriolar-targeting region of Cep63. The paradox raises the possibility that other proteins may function redundantly with Cep57 to recruit Cep63 and Cep152.

Cep57l1 forms a complex with Cep63 and Cep152 at the proximal end of mother centrioles

Cep57l1, the paralog of Cep57, has been reported to function in the anterior and posterior cruciate ligaments of the knees (Liu et al., 2015). Cep57l1 has similar function domains and has an ∼43% identity to Cep57 (Fig. 3A; Fig. S3). We hypothesized that Cep57l1 might localize at the centriole and function redundantly with Cep57 to recruit the Cep63–Cep152 complex. We first tested whether Cep57l1 also interacts with Cep63 as Cep57. We found that the N-terminus of Cep57l1 was necessary and sufficient to bind Cep63 (Fig. 3B,C,G). Cep63 also interacted with Cep57l1 through its N-terminal centrosomal-targeting fragment (Fig. 3E–G).

Owing to the lack of an anti-Cep57l1 antibody, we examined the subcellular localization of Cep57l1 by expressing GFP–Cep57l1 in U2OS cells. GFP–Cep57l1 also formed a ring-like structure with Cep63 and Cep152 at the proximal end of centrioles during interphase with a diameter comparable to that of the Cep57 rings (227±33 nm, 44 centrioles from 24 cells) (Fig. 3D). GFP–Cep57l1, however, did not form bundled filaments (Fig. 3D,H). Although both the N- and C-termini of Cep57l1 localized to the centriole, their fluorescence intensities were weaker by at least 4-fold as compared to that of full-length Cep57l1 (Fig. 3D; Fig. S4A), indicating that both regions are required for the strong centriolar localization of Cep57l1.

In multiciliated mTECs, GFP–Cep57l1 displayed a similar subcellular distribution to that of Cep57 and Cep63 (Fig. 3I versus Fig. 1E–G) (Zhao et al., 2013). It also specifically associated with the parental centrioles but not with deuterosomes at the early stages of centriole amplification in mTECs (stages II and III) (Fig. 3I). In stage IV, GFP–Cep57l1 started to accumulate at the base of nascent centrioles to form a goblet-like structure (Fig. 3I). Like Cep57, GFP–Cep57l1 still localized at the proximal end of centrioles in a ring-like pattern in stages V and VI. Collectively, these findings imply that Cep57l1 interacts with Cep63 at the proximal end of centrioles.

Cep57 and its paralog Cep57l1 function redundantly to recruit the Cep63–Cep152 complex for centriole duplication

To examine whether Cep57l1 is required for the localization of Cep63 and Cep152, we depleted Cep57l1 by RNAi in both wild-type and *Cep57* KO U2OS cells (Fig. 4). Given the lack of an anti-Cep57l1 antibody, we selected Cep57l1 siRNA oligonucleotides by monitoring the GFP–Cep57l1 signal when co-expressed with various siRNA oligonucleotides, and two oligonucleotides, 57l1i-1 and 57l1i-2, were chosen based on knockdown efficiency (Fig. S4B).

In contrast to what is seen upon the depletion of Cep57 (Watanabe et al., 2019), the depletion of Cep57l1 did not affect the integrity of PCM (Fig. S4C). In addition, and similar to what is seen with Cep57 deficiency (Fig. 2H,I), the depletion of Cep57l1 alone did not impair the centriolar localization of Cep63 or Cep152 in control U2OS cells (Fig. 4A). The double depletion of Cep57 and Cep57l1, however, significantly reduced the centriolar localization of Cep63 and Cep152 (Fig. 4B). Furthermore, the centriolar localization of Cep63 and Cep152 was rescued by expressing either GFP–Cep57 or an siRNA-resistant GFP–Cep57l1 (GFP–Cep57l1R), but not GFP–centrin1 (GFP–Cetn1) (Fig. 4C,D). Therefore, Cep57 and Cep57l1 function redundantly to ensure the centriolar localization of the Cep63–Cep152 complex.

Journal of Cell Science (2020) 133, jcs241836. doi:10.1242/jcs.241836

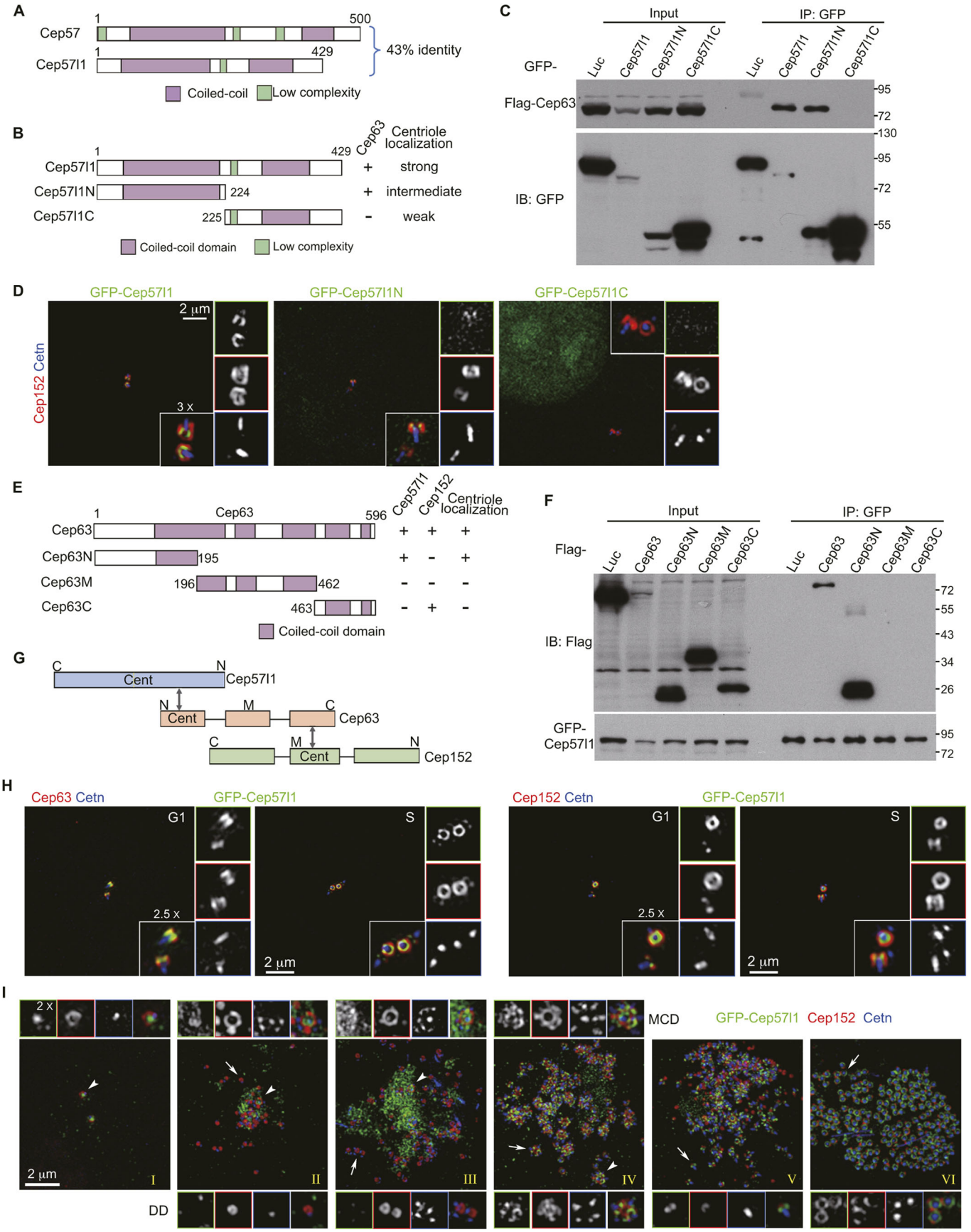

Fig. 3. See next page for legend.

Fig. 3. Cep57l1, the paralog of Cep57, forms a complex with Cep63 and Cep152 at the proximal end of centrioles. (A) Schematic diagram of mouse Cep57 and its paralog Cep57l1. (B) Schematic diagram of Cep57l1 and deletion mutants showing the ability to interact with Cep63 and to localize to the centriole. (C) Mapping the Cep63-interacting domain of Cep57l1. GFP-tagged Cep57l1 or its mutants were co-expressed with Flag–Cep63 in HEK 293T cells. Co-immunoprecipitation was then performed with GFP beads. Luc , luciferase control. (D) The requirement of full-length Cep57l1 for its centriolar localization. U2OS cells expressing GFP-tagged Cep57 or deletion mutants for 48 h were pre-extracted with 0.5% Triton X-100 for 40 s and co-stained with Cep152 (red) and Cetn (blue). Note that the centrosomal localization of both N- and C-terminal deletion mutants is much weaker than that of the full-length Cep57l1. (E) Schematic diagram of Cep63 and deletion mutants showing the ability to interact with Cep57l1 and Cep152 and to localize to the centriole. (F) Mapping of the Cep57l1-interacting regions of Cep63. GFP-tagged Cep57l1 was co-expressed with Flag-tagged Cep63 or mutants in HEK 293T cells. Co-Immunoprecipitation was then performed with GFP beads. Luc, luciferase control. (G) Schematics showing the interaction relationship of Cep57l1, Cep63 and Cep152. Cent represents the centriolar-targeting region. (H) GFP–Cep57l1 colocalizes with Cep63 and Cep152 at the proximal end of centrioles in U2OS cells. GFP–Cep57l1 was transiently expressed in human U2OS cells, and cells were also co-stained for Cetn and Cep63 (left) or Cep152 (right). (I) The subcellular localization of GFP–Cep57l1 during centriole amplification in mTECs. Representative 3D-SIM images were acquired from mTECs at day 3 after inducing multiciliation with the air-liquid interface system (ALI d3). Magnified areas show details for MCD (above; indicated by arrowheads) and DD (below; indicated by arrows) pathway centriole amplification.

To investigate whether the co-depletion of Cep57 and Cep57l1 interferes with procentriole assembly, we pulse-labeled S-phase cells with EdU, and examined procentrioles marked by Sas-6 in the EdU-positive cells. We observed a marked reduction in procentriole biogenesis in the co-depleted cells (Fig. 4E), demonstrating a critical function of Cep57 and Cep57l1 in the initiation of centriole duplication.

In this study, we find that Cep57 and its paralog Cep57l1 localize to the proximal end of parental centrioles and function redundantly to recruit the Cep63–Cep152 complex. Co-depletion of Cep57 and Cep57l1 disrupts the centriolar localization of the Cep63–Cep152 complex and consequently inhibits normal procentriole biogenesis in S-phase cells. They appear to play similar roles in the parental centriole-mediated centriole amplification in multiciliated cells (Figs 1E–G and 3I). Interestingly, their strong basal body localization (Figs 1E–G and 3I) also implies that they have roles in multicilia formation and function, which should be clarified in the future.

Recently, Cep295 has been identified as the key protein for the conversion of daughter centrioles into functional mother centrioles, and the loading of Cep152 by Cep135 and Cep295 to daughter centrioles is critical for the conversion (Fu et al., 2016; Izquierdo et al., 2014; Tsuchiya et al., 2016). Interestingly, Cep295 is only required for targeting of Cep152 to the young mother centriole, but not to the old mother centriole, implying that other scaffold proteins might play a role in anchoring Cep152 to the old mother centriole. Our findings here raise a possibility that Cep63 recruited by Cep57 and/or Cep57l1 may function in detaining Cep152 at the mother centriole after its initial loading by Cep135–Cep295 during the centriole-to-centrosome conversion. In the future, it will be interesting to investigate the relationship among Cep57 and Cep57l1, Cep63 and Cep295 in the centriolar localization of Cep152.

MATERIALS AND METHODS

Cell culture, transfection, RNAi and viral infection

mTECs were isolated from 4-week C57BL/6J mice and cultured as described previously (Zhao et al., 2013). Experiments involving mouse tissues were performed in accordance with protocols approved by the Institutional Animal Care and Use Committee of Institute of Biochemistry and Cell Biology. U2OS (HTB-96, ATCC) and HEK 293T (CRL-11268, ATCC) cells were cultured in Dulbecco's modified Eagle's medium (DMEM) supplemented with 10% fetal bovine serum (FBS, Thermo Fisher Scientific) at 37°C and 5% CO_2. Cells were routinely tested for mycoplasma contamination by PCR. For U2OS cells, plasmids were transfected using Lipofectamine 2000 according to the manufacturer's instructions (ThermoFisher). For ectopic protein expression and lentiviral production in HEK 293T cells, plasmids were transfected by the calcium phosphate method. To observe the process of centriole amplification, mTECs were harvested at day 3 after the air-liquid interface (ALI) culture, and lentiviral infection of mTECs was performed as described previously (Zhao et al., 2013). Human Cep57l1 protein was depleted using two different siRNA duplex oligonucleotides that targeted the sequences 5′-CGTTGTACTCT-TCTAGAGA-3′ (57l1i-1) and 5′-GCTTCAAACTGGACTTGAA-3′ (57l-1i-2). A non-targeting siRNA duplex oligonucleotide was used as a control with the sequence 5′-TTCTCCGAACGTGTCACGTtt-3′ (Ctrli). U2OS cells were transfected with siRNA oligonucleotides using Lipofectamine RNAi-MAX reagent (Thermo Fisher Scientific) for 48 h. To improve the efficiency of knockdown, a second round of siRNA transfection was conducted for another 48 h.

Plasmids

Full-length mouse cDNAs of Cep57 (NM_026665), Cep63 (NM_001301689), and Cep57l1 (NM_029132), centrin1 (NM_007593) and PCNT (1485-2896 aa, NM_001282992) were amplified from mTEC cDNA by PCR amplification. Full-length human cDNAs of Cep57 (NM_014679) and Cep57l1 (NM_173830) were amplified from HEK 293T cDNA and the fragments were subcloned into pEGFP-C1 (Clontech, 632470). For ectopic expression, fragments of the indicated regions of mouse Cep57, Cep63 and Cep57l1 were made by PCR amplification of and cloned into pEGFP-C1 or pcDNA3.1-NFLAG [a version of pcDNA3.1 (ThermoFisher, V79020), modified to encode the FLAG tag], respectively. To express RFP–centrin1, the full-length of centrin1 was cloned into pLV-RFP (generated by replacing the GFP cassette in pLV-GFP with an RFP cassette; kindly provided by Dr Q. Zhai, Shanghai Institutes for Biological Sciences, Chinese Academy of Sciences). To infect mTECs, Cep57 or Cep57l1 were cloned into pLV-GFP (kindly provided by Dr Q. Zhai). For rescue experiments, RNAi-resistant GFP–Cep57l1 (GFP–Cep57l1R) was made by site-directed mutagenesis of pEGFP-Cep57l1. For antibody production, the full-length of mouse Cep57 and Cep152 [amino acids (aa) 1–735] were cloned into pGEX-4T-1 (GE Healthcare, 27-1542-01) to express GST-tagged proteins, and the PCNT (aa 1485–2896) fragment was cloned into pET-32a (Novagen, 69015) to express His-tagged proteins. All constructs were verified by sequencing.

GST pulldown assay

GST and GST–Cep57 were purified with glutathione–agarose beads (Sigma, G4510). His–Cep63 and His–Cep152M were purified with Ni-NTA agarose beads (Qiagen, 30230). *In vitro* GST pulldown assays were performed by incubating recombinant proteins in lysis buffer [500 mM NaCl, 50 mM HEPES-KOH pH 7.8, 5 mM EDTA, 3 mM DTT, 0.5 mM PMSF and complete protease inhibitors (Sigma, 539134)] for 4 h at 4°C. After three washes with lysis buffer, proteins were eluted with SDS-PAGE sample buffer and analyzed by SDS-PAGE.

Generation of knockout cell lines

The Cep57- and Cep63-knockout U2OS cell lines were generated by the CRISPR/Cas9-mediated gene editing system (Cong et al., 2013). The sequences of sgRNAs were Cep57 (5′-CACAAGCCCTAGCCATGCCG-3′), Cep63 (5′-AACATGCTGTAGAAGCTATA-3′) and Scramble (5′-GCACTACCAGAGCTAACTCA-3′). The synthesized primers were annealed and inserted into pLV-Cas9-puromycin vector.

U2OS cells were transfected with the plasmids for 48 h and were treated with 1.5 µg/ml Puromycin (Sigma, P8833) for 10 days. The cells were then serially diluted and single colonies were examined by immunofluorescence microscopy to confirm the loss of the indicated proteins. Genomic DNAs isolated from the selected cells were PCR amplified with the following primers: Cep57-p (5′-GTGGTGTAGAGAATATAACTTCAAT-3′), Cep57-r (5′-CTCGATCATTGC ACAAAGCTTTACT-3′), Cep63-p (5′-CTCAT-

Journal of Cell Science (2020) 133, jcs241836. doi:10.1242/jcs.241836

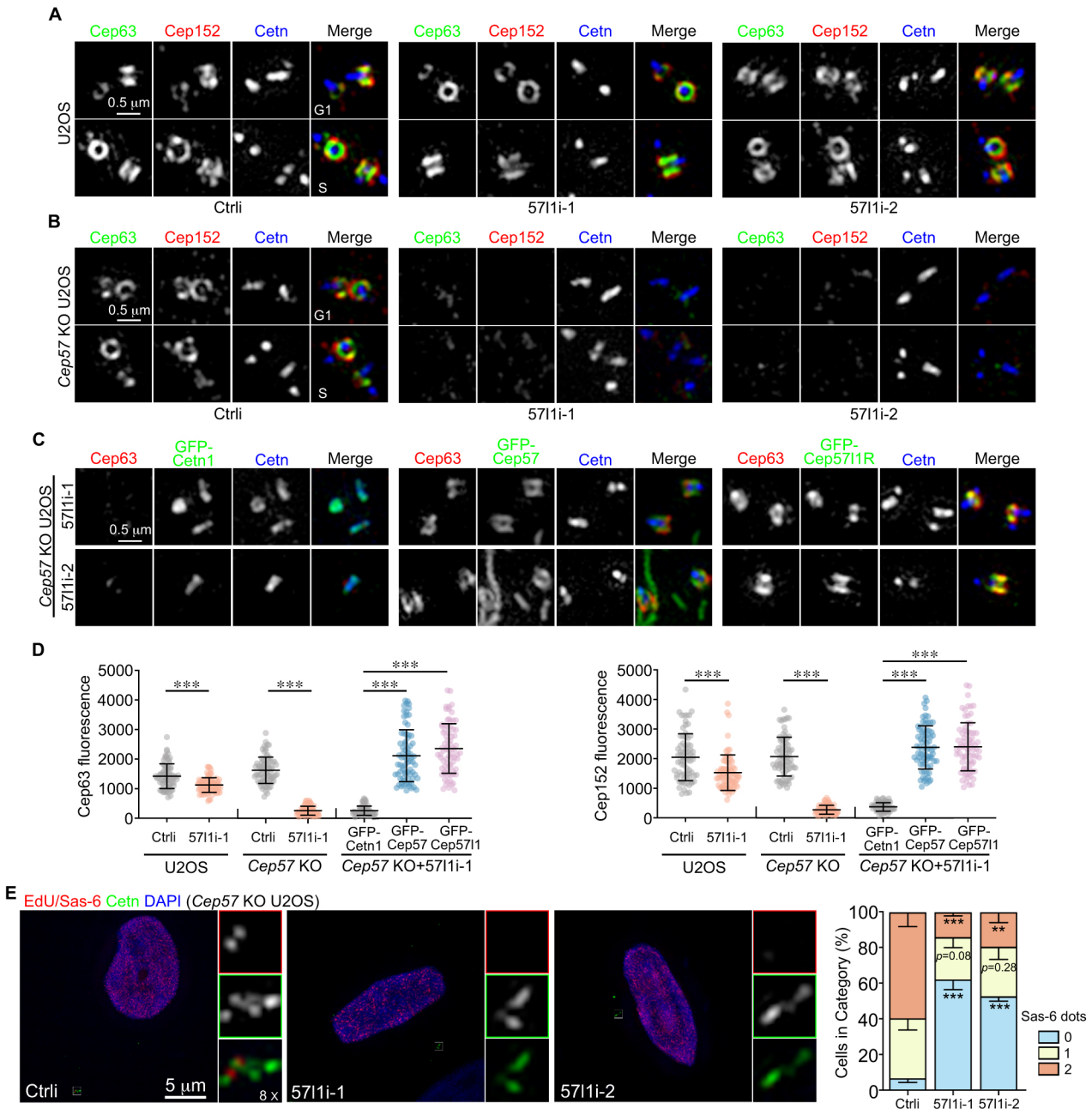

Fig. 4. Cep57 and Cep57l1 recruit the Cep63-Cep152 complex for centriole duplication. (A,B) Centriolar localization of Cep63 and Cep152 was markedly reduced upon depletion of both Cep57 and Cep57l1 but not Cep57l1 alone. Intact U2OS cells (A) or *Cep57* KO U2OS cells (B) were transfected with a control (Ctrli) or Cep57l1 (57l1i-1 or 57l1i-2) siRNA oligonucleotide, followed by immunofluorescence analysis. (C) Expression of either GFP-tagged Cep57 or a siRNA-resistant Cep57l1 (Cep57l1R) rescued the co-depletion-induced centriolar loss of Cep63 and Cep152. *Cep57* KO U2OS cells expressing GFP-tagged Cetn1, Cep57 or Cep57l1R were co-transfected with 57l1i-1 or 57l1i-2 for 48 h and fixed for immunofluorescence analysis. (D) Centriolar intensities of Cep63 and Cep152 in (A–C). 75 G1-phase cells from three independent experiments were used for the measurement in each group. Unpaired Student's *t*-test: ***P<0.001. Mean±s.d. values are presented in the plots. (E) Co-depletion of Cep57 and Cep57l1 repressed procentriole formation. *Cep57* knockout cells were transfected with a Ctrli or Cep57l1 oligonucleotide and stained for Sas-6 and Cetn. EdU was used to label S-phase cells. Quantification results were from three independent experiments; 100 EdU-positive cells were scored in each experiment and condition. Error bars represent s.d. **P<0.01; ***P<0.001 (two tailed *t*-test against the corresponding Ctrli groups).

ACATGAGGCCAGAATACAAA-3′) and Cep63-r (5′-GCCTAGTGCT-TAATACCTAGTCATT-3′). The PCR products were cloned into a TA-cloning vector and for each KO cell line, six clones were picked for sequencing.

Immunoprecipitations

Co-immunoprecipitation was performed as described previously (Zhao et al., 2013). In brief, HEK293T cells were transiently transfected, cultured for 48 h, washed with PBS and lysed in lysis buffer [500 mM NaCl, 50 mM HEPES-KOH pH 7.8, 5 mM EDTA, 3 mM DTT, 0.5 mM PMSF and complete protease inhibitors (Sigma, 539134)]. Lysates were further cleared by centrifugation at 14,000 ***g*** and subjected to co-immunoprecipitations using anti-Flag agarose beads (Sigma, A2220) or GFP-Trap agarose beads (Chromotek, gat-20). Beads were washed with lysis buffer, eluted in SDS-loading buffer and run on SDS-PAGE gels.

Antibodies

The following primary antibodies were used for western blotting in this study: mouse monoclonal antibodies against Flag (Sigma, F3165, 1:5000), His (Sigma, H1029, 1:3000) and β-actin (Sigma, A5316, 1:5000); rabbit antibodies against Cep63 (Millipore, 06-1292, 1:2000), GFP (Proteintech, 50430-2-AP, 1:2000) and GST (Shanghai Wolwo biotech, Mab-GS01, 1:3000). Secondary antibodies were HRP-conjugated goat anti-mouse IgG (H+L) (ThermoFisher, G21040, 1:5000) and goat anti-rabbit IgG (H+L) (ThermoFisher, G21243, 1:5000).

Primary antibodies purchased for immunostaining were: chicken antibody against GFP (ThermoFisher, A10262, 1:200); mouse antibodies against centrin (Millipore, 04-1624, 1:200), acetylated tubulin (Sigma, T6793, 1:1000), α-tubulin (Sigma, T5168, 1:1000) and Sas-6 (Santa Cruz Biotechnology, sc-81431, 1:50); and rabbit antibody against CP110 (Proteintech, 12780-1-AP, 1:200) and Cep63 (Millipore, 06-1292, 1:200). Rabbit anti-PCNT (against 1485–2896 aa of mouse PCNT, 1:200), chicken anti-Cep152 (against 1–735 aa of mouse Cep152, 1:300) and rat anti-Cep57 (against full-length of mouse Cep57, 1:200) polyclonal antibodies were generated with purified GST- or His-tagged proteins (Abclonal). The following secondary antibodies purchased from ThermoFisher were used for immunofluorescence: goat anti-mouse IgG (H+L) Alexa Fluor 405 (A-31553, 1:200), goat anti-rabbit IgG (H+L) Alexa Fluor 405 (A-31556, 1:200), donkey anti-rabbit IgG (H+L) Alexa Fluor 488 (A-21206, 1:1000), goat anti-chicken IgY Alexa Fluor 488 (A-11039, 1:1000), goat anti-chicken IgY Alexa Fluor 546 (A-11040, 1:1000), goat anti-rat IgG (H+L) Alexa Fluor 546 (A-11081, 1:1000), and goat anti-rabbit IgG (H+L) Alexa Fluor 546 (A-11035, 1:1000).

Fluorescence microscopy

For immunofluorescence experiments, mTECs were pre-extracted with 0.5% Triton X-100 in PBS for 3 min before fixation with 4% fresh paraformaldehyde in PBS for 15 min at room temperature. For U2OS cells grown on coverslips, cells were pre-extracted with 0.5% Triton X-100 in PBS for 40 s and then fixed with 4% paraformaldehyde in PBS for 15 min at room temperature. After fixation, cells were permeabilized with 0.5% Triton X-100 in PBS for 15 min and blocked with blocking buffer (4% BSA in PBS) for 1 h. The incubation with primary and secondary antibodies was performed at room temperature for 2 h and 1 h, respectively. 3D-SIM images were collected on the DeltaVision OMX V3 imaging system (GE Healthcare). The setting of the OMX V3 system was as described previously (Zhao et al., 2013). Confocal images were captured with the Leica TCS SP8 microsystem with a 100×/1.40 NA oil immersion objective at 400-nm intervals. Serial images were processed with maximum intensity projections.

Quantification and statistical analysis

Images of each grouped sample were captured under the same condition (gain, offset, exposure time, pixel size and laser settings). The fluorescence intensity and the diameters of the indicated proteins were measured with Photoshop (Adobe) and Image J (Fiji), respectively. Statistical results are presented as mean±s.d. Two-tailed Student's *t*-test (GraphPad Prism software) was used to calculate *P*-values between unpaired samples. Differences were considered significant when $P<0.05$.

Acknowledgements

The authors thank the Centre for Biological Imaging, Institute of Biophysics, CAS, for support on 3D-SIM imaging, and institutional core facilities for cell biology and molecular biology for instrumental and technical support.

Competing interests

The authors declare no competing or financial interests.

Author contributions

Conceptualization: H.Z., X.Z., X.Y.; Methodology: H.Z.; Validation: S.Y., Q.C.; Investigation: H.Z., X.D., Q.C.; Resources: G.L., Q.H.; Writing - original draft: H.Z., X.Y.; Writing - review & editing: H.Z., X.Z., X.Y.; Visualization: H.Z., X.Y.; Supervision: X.Z., X.Y.; Project administration: X.Z., X.Y.; Funding acquisition: X.Z.

Funding

This work was supported by the National Natural Science Foundation of China (31991192 to X.Z.) and the Chinese Academy of Sciences (XDB19020000).

Supplementary information

Supplementary information available online at
https://jcs.biologists.org/lookup/doi/10.1242/jcs.241836.supplemental

Peer review history

The peer review history is available online at
https://jcs.biologists.org/lookup/doi/10.1242/jcs.241836.reviewer-comments.pdf

References

Arquint, C., Sonnen, K. F., Stierhof, Y.-D. and Nigg, E. A. (2012). Cell-cycle-regulated expression of STIL controls centriole number in human cells. *J. Cell Sci.* **125**, 1342-1352. doi:10.1242/jcs.099887

Arquint, C., Gabryjonczyk, A.-M., Imseng, S., Böhm, R., Sauer, E., Hiller, S., Nigg, E. A. and Maier, T. (2015). STIL binding to Polo-box 3 of PLK4 regulates centriole duplication. *eLife* **4**, e07888. doi:10.7554/eLife.07888

Azimzadeh, J. and Marshall, W. F. (2010). Building the centriole. *Curr. Biol.* **20**, R816-R825. doi:10.1016/j.cub.2010.08.010

Bettencourt-Dias, M., Hildebrandt, F., Pellman, D., Woods, G. and Godinho, S. A. (2011). Centrosomes and cilia in human disease. *Trends Genet.* **27**, 307-315. doi:10.1016/j.tig.2011.05.004

Bossard, C., Laurell, H., Van den Berghe, L., Meunier, S., Zanibellato, C. and Prats, H. (2003). Translokin is an intracellular mediator of FGF-2 trafficking. *Nat. Cell Biol.* **5**, 433-439. doi:10.1038/ncb979

Brito, D. A., Gouveia, S. M. and Bettencourt-Dias, M. (2012). Deconstructing the centriole: structure and number control. *Curr. Opin. Cell Biol.* **24**, 4-13. doi:10.1016/j.ceb.2012.01.003

Brown, N. J., Marjanović, M., Lüders, J., Stracker, T. H. and Costanzo, V. (2013). Cep63 and cep152 cooperate to ensure centriole duplication. *PLoS ONE* **8**, e69986. doi:10.1371/journal.pone.0069986

Carvalho-Santos, Z., Machado, P., Alvarez-Martins, I., Gouveia, S. M., Jana, S. C., Duarte, P., Amado, T., Branco, P., Freitas, M. C., Silva, S. T. N. et al. (2012). BLD10/CEP135 is a microtubule-associated protein that controls the formation of the flagellum central microtubule pair. *Dev. Cell* **23**, 412-424. doi:10.1016/j.devcel.2012.06.001

Cizmecioglu, O., Arnold, M., Bahtz, R., Settele, F., Ehret, L., Haselmann-Weiss, U., Antony, C. and Hoffmann, I. (2010). Cep152 acts as a scaffold for recruitment of Plk4 and CPAP to the centrosome. *J. Cell Biol.* **191**, 731-739. doi:10.1083/jcb.201007107

Comartin, D., Gupta, G. D., Fussner, E., Coyaud, E., Hasegan, M., Archinti, M., Cheung, S. W. T., Pinchev, D., Lawo, S., Raught, B. et al. (2013). CEP120 and SPICE1 cooperate with CPAP in centriole elongation. *Curr. Biol.* **23**, 1360-1366. doi:10.1016/j.cub.2013.06.002

Cong, L., Ran, F. A., Cox, D., Lin, S., Barretto, R., Habib, N., Hsu, P. D., Wu, X., Jiang, W., Marraffini, L. A. et al. (2013). Multiplex genome engineering using CRISPR/Cas systems. *Science* **339**, 819-823. doi:10.1126/science.1231143

Cuevas, R., Korzeniewski, N., Tolstov, Y., Hohenfellner, M. and Duensing, S. (2013). FGF-2 disrupts mitotic stability in prostate cancer through the intracellular trafficking protein CEP57. *Cancer Res.* **73**, 1400-1410. doi:10.1158/0008-5472.CAN-12-1857

Dzhindzhev, N. S., Yu, Q. D., Weiskopf, K., Tzolovsky, G., Cunha-Ferreira, I., Riparbelli, M., Rodrigues-Martins, A., Bettencourt-Dias, M., Callaini, G. and Glover, D. M. (2010). Asterless is a scaffold for the onset of centriole assembly. *Nature* **467**, 714-718. doi:10.1038/nature09445

Firat-Karalar, E. N., Rauniyar, N., Yates, J. R., III and Stearns, T. (2014). Proximity interactions among centrosome components identify regulators of centriole duplication. *Curr. Biol.* **24**, 664-670. doi:10.1016/j.cub.2014.01.067

Fu, J., Lipinszki, Z., Rangone, H., Min, M., Mykura, C., Chao-Chu, J., Schneider, S., Dzhindzhev, N. S., Gottardo, M., Riparbelli, M. G. et al. (2016). Conserved molecular interactions in centriole-to-centrosome conversion. *Nat. Cell Biol.* **18**, 87-99. doi:10.1038/ncb3274

Gönczy, P. (2015). Centrosomes and cancer: revisiting a long-standing relationship. *Nat. Rev. Cancer* **15**, 639-652. doi:10.1038/nrc3995

Hatch, E. M., Kulukian, A., Holland, A. J., Cleveland, D. W. and Stearns, T. (2010). Cep152 interacts with Plk4 and is required for centriole duplication. *J. Cell Biol.* **191**, 721-729. doi:10.1083/jcb.201006049

Hung, L.-Y., Chen, H.-L., Chang, C.-W., Li, B.-R. and Tang, T. K. (2004). Identification of a novel microtubule-destabilizing motif in CPAP that binds to tubulin heterodimers and inhibits microtubule assembly. *Mol. Biol. Cell* **15**, 2697-2706. doi:10.1091/mbc.e04-02-0121

Izquierdo, D., Wang, W.-J., Uryu, K. and Tsou, M.-F. B. (2014). Stabilization of cartwheel-less centrioles for duplication requires CEP295-mediated centriole-to-centrosome conversion. *Cell Rep.* **8**, 957-965. doi:10.1016/j.celrep.2014.07.022

Kim, T.-S., Park, J.-E., Shukla, A., Choi, S., Murugan, R. N., Lee, J. H., Ahn, M., Rhee, K., Bang, J. K., Kim, B. Y. et al. (2013). Hierarchical recruitment of Plk4 and regulation of centriole biogenesis by two centrosomal scaffolds, Cep192 and Cep152. *Proc. Natl. Acad. Sci. USA* **110**, E4849-E4857. doi:10.1073/pnas.1319656110

Kim, T.-S., Zhang, L., Il Ahn, J., Meng, L., Chen, Y., Lee, E., Bang, J. K., Lim, J. M., Ghirlando, R., Fan, L. et al. (2019). Molecular architecture of a cylindrical

self-assembly at human centrosomes. *Nat. Commun.* **10**, 1151. doi:10.1038/s41467-019-08838-2

Kohlmaier, G., Lončarek, J., Meng, X., McEwen, B. F., Mogensen, M. M., Spektor, A., Dynlacht, B. D., Khodjakov, A. and Gönczy, P. (2009). Overly long centrioles and defective cell division upon excess of the SAS-4-related protein CPAP. *Curr. Biol.* **19**, 1012-1018. doi:10.1016/j.cub.2009.05.018

Lin, Y.-C., Chang, C.-W., Hsu, W.-B., Tang, C.-J. C., Lin, Y.-N., Chou, E.-J., Wu, C.-T. and Tang, T. K. (2013a). Human microcephaly protein CEP135 binds to hSAS-6 and CPAP, and is required for centriole assembly. *EMBO J.* **32**, 1141-1154. doi:10.1038/emboj.2013.56

Lin, Y.-N., Wu, C.-T., Lin, Y.-C., Hsu, W.-B., Tang, C.-J. C., Chang, C.-W. and Tang, T. K. (2013b). CEP120 interacts with CPAP and positively regulates centriole elongation. *J. Cell Biol.* **202**, 211-219. doi:10.1083/jcb.201212060

Liu, Y., Li, Y., March, M. E., Nguyen, K., Xu, K., Wang, F., Guo, Y., Keating, B., Glessner, J., Li, J. et al. (2015). Copy number variation in CEP57L1 predisposes to congenital absence of bilateral ACL and PCL ligaments. *Hum. Genomics* **9**, 31. doi:10.1186/s40246-015-0053-z

Loncarek, J. and Bettencourt-Dias, M. (2018). Building the right centriole for each cell type. *J. Cell Biol.* **217**, 823-835. doi:10.1083/jcb.201704093

Lukinavičius, G., Lavogina, D., Orpinell, M., Umezawa, K., Reymond, L., Garin, N., Gönczy, P. and Johnsson, K. (2013). Selective chemical crosslinking reveals a Cep57-Cep63-Cep152 centrosomal complex. *Curr. Biol.* **23**, 265-270. doi:10.1016/j.cub.2012.12.030

Meunier, S., Navarro, M. G.-J., Bossard, C., Laurell, H., Touriol, C., Lacazette, E. and Prats, H. (2009). Pivotal role of translokin/CEP57 in the unconventional secretion versus nuclear translocation of FGF2. *Traffic* **10**, 1765-1772. doi:10.1111/j.1600-0854.2009.00985.x

Momotani, K., Khromov, A. S., Miyake, T., Stukenberg, P. T. and Somlyo, A. V. (2008). Cep57, a multidomain protein with unique microtubule and centrosomal localization domains. *Biochem. J.* **412**, 265-273. doi:10.1042/BJ20071501

Moyer, T. C., Clutario, K. M., Lambrus, B. G., Daggubati, V. and Holland, A. J. (2015). Binding of STIL to Plk4 activates kinase activity to promote centriole assembly. *J. Cell Biol.* **209**, 863-878. doi:10.1083/jcb.201502088

Nigg, E. A. and Holland, A. J. (2018). Once and only once: mechanisms of centriole duplication and their deregulation in disease. *Nat. Rev. Mol. Cell Biol.* **19**, 297-312. doi:10.1038/nrm.2017.127

Nigg, E. A. and Raff, J. W. (2009). Centrioles, centrosomes, and cilia in health and disease. *Cell* **139**, 663-678. doi:10.1016/j.cell.2009.10.036

Ohta, M., Ashikawa, T., Nozaki, Y., Kozuka-Hata, H., Goto, H., Inagaki, M., Oyama, M. and Kitagawa, D. (2014). Direct interaction of Plk4 with STIL ensures formation of a single procentriole per parental centriole. *Nat. Commun.* **5**, 5267. doi:10.1038/ncomms6267

Ohta, M., Watanabe, K., Ashikawa, T., Nozaki, Y., Yoshiba, S., Kimura, A. and Kitagawa, D. (2018). Bimodal binding of STIL to Plk4 controls proper centriole copy number. *Cell Rep.* **23**, 3160-3169.e4. doi:10.1016/j.celrep.2018.05.030

Schmidt, T. I., Kleylein-Sohn, J., Westendorf, J., Le Clech, M., Lavoie, S. B., Stierhof, Y.-D. and Nigg, E. A. (2009). Control of centriole length by CPAP and CP110. *Curr. Biol.* **19**, 1005-1011. doi:10.1016/j.cub.2009.05.016

Sieben, C., Banterle, N., Douglass, K. M., Gönczy, P. and Manley, S. (2018). Multicolor single-particle reconstruction of protein complexes. *Nat. Methods* **15**, 777-780. doi:10.1038/s41592-018-0140-x

Sir, J.-H., Barr, A. R., Nicholas, A. K., Carvalho, O. P., Khurshid, M., Sossick, A., Reichelt, S., D'Santos, C., Woods, C. G. and Gergely, F. (2011). A primary microcephaly protein complex forms a ring around parental centrioles. *Nat. Genet.* **43**, 1147-1153. doi:10.1038/ng.971

Snape, K., Hanks, S., Ruark, E., Barros-Núñez, P., Elliott, A., Murray, A., Lane, A. H., Shannon, N., Callier, P., Chitayat, D. et al. (2011). Mutations in CEP57 cause mosaic variegated aneuploidy syndrome. *Nat. Genet.* **43**, 527-529. doi:10.1038/ng.822

Sonnen, K. F., Gabryjonczyk, A.-M., Anselm, E., Stierhof, Y.-D. and Nigg, E. A. (2013). Human Cep192 and Cep152 cooperate in Plk4 recruitment and centriole duplication. *J. Cell Sci.* **126**, 3223-3233. doi:10.1242/jcs.129502

Tsuchiya, Y., Yoshiba, S., Gupta, A., Watanabe, K. and Kitagawa, D. (2016). Cep295 is a conserved scaffold protein required for generation of a bona fide mother centriole. *Nat. Commun.* **7**, 12567. doi:10.1038/ncomms12567

Watanabe, K., Takao, D., Ito, K. K., Takahashi, M. and Kitagawa, D. (2019). The Cep57-pericentrin module organizes PCM expansion and centriole engagement. *Nat. Commun.* **10**, 931. doi:10.1038/s41467-019-08862-2

Wu, Q., He, R., Zhou, H., Yu, A. C. H., Zhang, B., Teng, J. and Chen, J. (2012). Cep57, a NEDD1-binding pericentriolar material component, is essential for spindle pole integrity. *Cell Res.* **22**, 1390-1401. doi:10.1038/cr.2012.61

Zhao, H., Zhu, L., Zhu, Y., Cao, J., Li, S., Huang, Q., Xu, T., Huang, X., Yan, X. and Zhu, X. (2013). The Cep63 paralogue Deup1 enables massive de novo centriole biogenesis for vertebrate multiciliogenesis. *Nat. Cell Biol.* **15**, 1434-1444. doi:10.1038/ncb2880

Zhao, H., Chen, Q., Fang, C., Huang, Q., Zhou, J., Yan, X. and Zhu, X. (2019). Parental centrioles are dispensable for deuterosome formation and function during basal body amplification. *EMBO Rep.* **20**, e46735. doi:10.15252/embr.201846735

Zhou, H., Wang, T., Zheng, T., Teng, J. and Chen, J. (2016). Cep57 is a Mis12-interacting kinetochore protein involved in kinetochore targeting of Mad1-Mad2. *Nat. Commun.* **7**, 10151. doi:10.1038/ncomms10151

Fig. S1, Zhao et al.

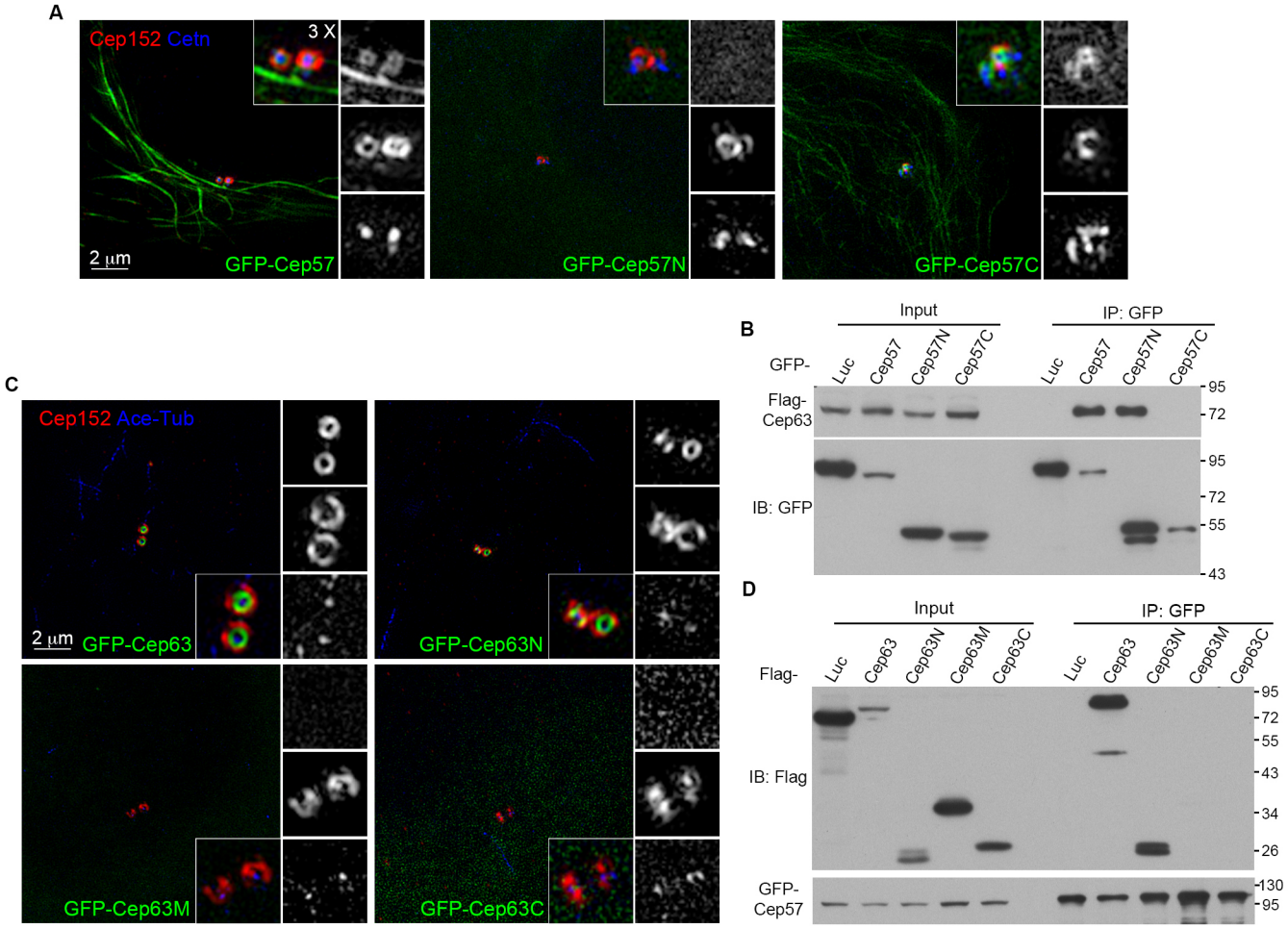

Figure S1. Domain mapping of Cep57 and Cep63.

(A) The C-terminus of Cep57 was required and sufficient for the centrosomal localization. U2OS cells expressing GFP-Cep57 or deletion mutants for 48 h were pre-extracted with 0.5% TritonX-100 for 40 s and co-stained with Cep152 (red) and Cetn (blue). (B) Mapping the Cep63-interacting regions of Cep57. GFP-tagged Cep57 or mutants were co-expressed with Flag-Cep63 in HEK 293T cells for 48h and co-Immunoprecipitation was performed with GFP beads. The numbers indicate amino acid positions. The N-terminus of Cep57 was required for the interaction with Cep63 and the C-terminus for its centrosomal localization. (C) The N-terminus of Cep63 was sufficient for the centrosomal localization. U2OS cells expressing GFP tagged Cep63 or each fragment were co-stained with Cep152 (red) and acetylated Tubulin (blue). (D) Domain mapping of Cep63. GFP-tagged Cep57 was co-expressed with Flag-Cep63 or mutants in HEK 293T cells for 48h and co-Immunoprecipitation was performed with GFP beads. The numbers indicate amino acid positions. The N-terminus of Cep63 was required for the interaction with Cep57 and its centrosomal localization, whereas the C-terminus was required for interacting with Cep152.

Fig. S2, Zhao et al.

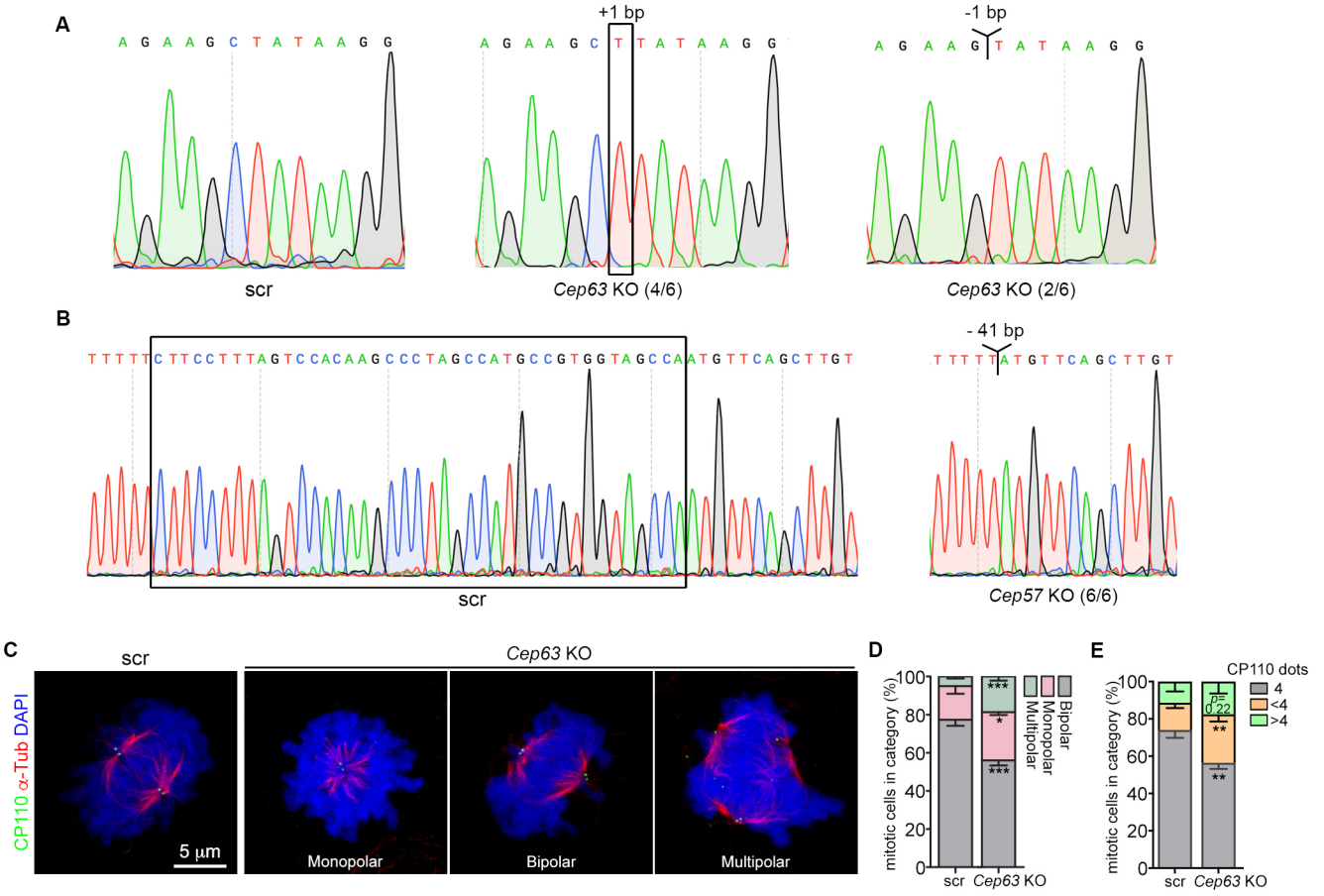

Figure S2. Sequencing and functional confirmation of *Cep63* or *Cep57* knockout cell lines.

(A,B) The frameshift mutations in the *Cep63* (A) or *Cep57* (B) knockout cell line. Genomic DNA from KO cells were PCR amplified and the amplicons were cloned into a TA-cloning vector. Six constructs of each cell line were sequenced. Both the insertion (4/6) and depletion mutations (2/6) introduced by CRISPR/Cas9 gene editing produced a premature termination at the position 307 amino acid of Cep63 in the *Cep63* knockout cells (A). All six constructs from the *Cep57* knockout cell line showed the same deletion mutation. The 41-bp deletion spanning exon 9 (31 bp) and its adjacent upstream intron (10 bp) of *Cep57* caused premature termination in the *Cep57* knockout cells(B). (C-E) The requirement of Cep63 for the proper mitotic spindle assembly and centriole duplication. *Cep63* knockout cells were fixed and stained with α-Tubulin (α-Tub, red), CP110 (green) antibodies and DAPI (blue). The frequency of spindle phenotypes (C,D) and the CP110 number (C,E) of control cells (scr) and *Cep63* knockout cells (*Cep63* KO) were scored from three independent experiments and subjected to unpaired Student's *t* test. 75 mitotic cells were scored per condition. Error bars represent standard deviations (s.d.). Student's *t* test: * P<0.05, ** P<0.01, and *** P<0.001.

Fig. S3, Zhao et al.

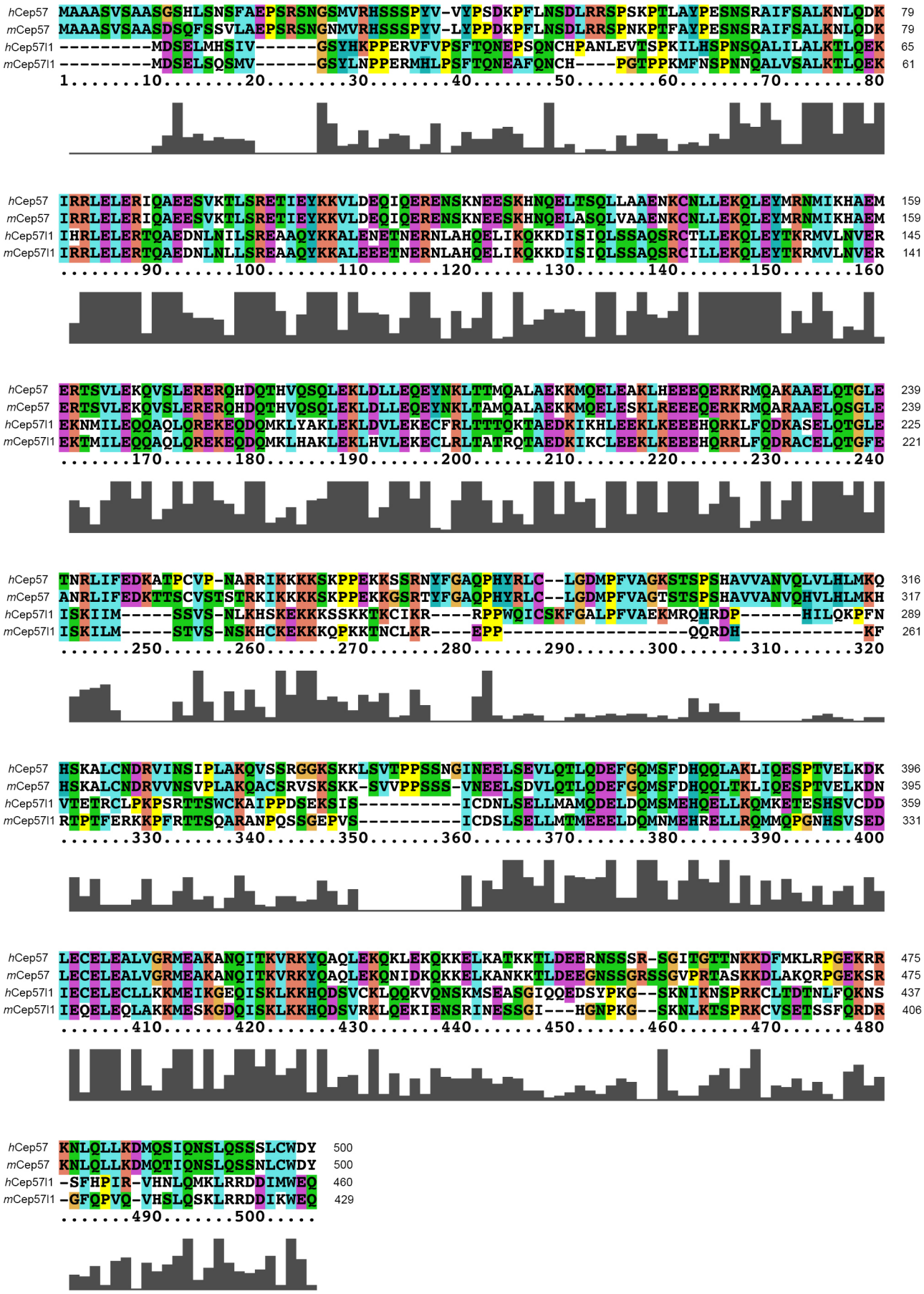

Figure S3. Sequence alignment of Cep57 and Cep57l1.

The proteins sequence alignment was generated with the Clustal X 2.0 software using default parameters. The protein sequences were obtained from GenBank (hCep57, NP_055494; mCep57, NP_080941, hCep57l1, NP_001077004 and mCep57l1, NP_083408).

Fig. S4, Zhao et al.

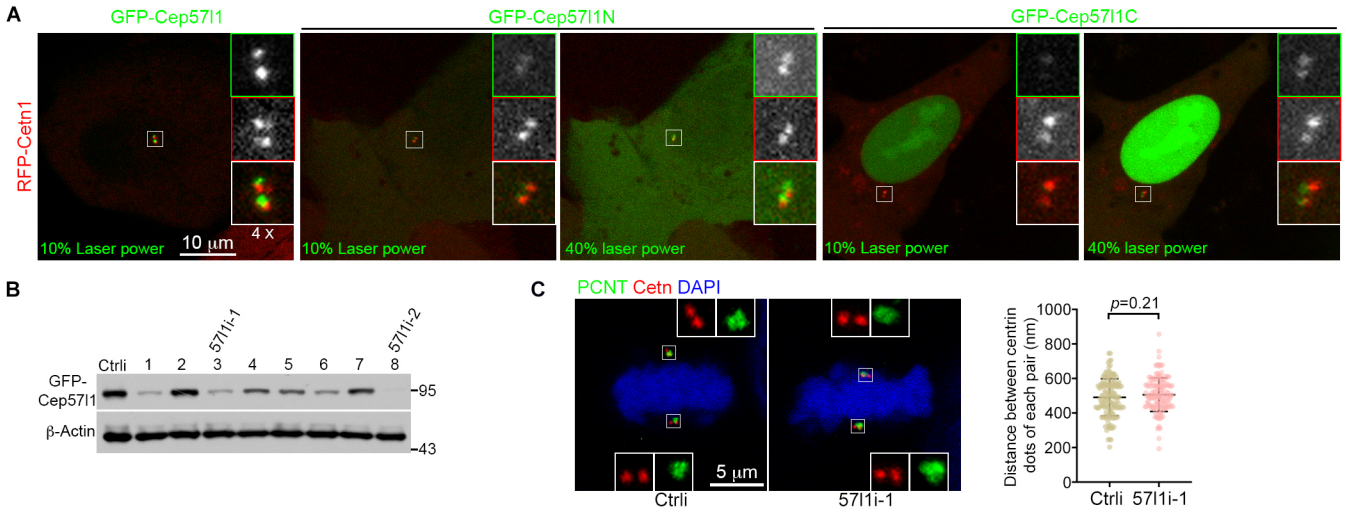

Figure S4. Functional analysis of Cep57l1.

(A) The requirement of full-length of Cep57l1 for its centriolar localization. U2OS cells expressing RFP-Centrin1 and GFP tagged Cep57l1 or deletion mutants were live imaged by Confocal (A). Note that the centrosomal localization of both N- and C-terminal deletion mutants is much weaker than that of the full-length Cep57l1. (B) Screening for siRNA oligos against human Cep57l1. HEK293T cells expressing GFP-Cep57l1 were con-transfected with a negative control siRNA oligo (Ctrli) or each indicated siRNA oligo (No. 1-8) for 48h and the cells were harvested for immunoblotting. β-Actin serves as the loading control. Three (No. 1, 3 and 8) out of the eight siRNA oligos dramatically reduced the expression of GFP-Cep57l1. Since No. 1 siRNA oligo also induced severe cell death, possibly due to off-target effects, No. 3 (which we termed 57l1i-1) and No. 8 (57l1i-2) oligos were used for the Cep57l1 knockdown experiments. (C) Cep57l1 was dispensable for the PCM organization. U2OS cells transfected with Ctrli or 57l1i-1 were stained with Cetn (red), Pericentrin (PCNT, green) antibodies and DAPI (blue). The distance between centrioles of each spindle pole were measured. Quantification results were from three independent experiments and subjected to unpaired Student's *t* test. 75 mitotic cells were scored per condition. Mean±s.d. values are presented in the plots.